SUPPORTING INFORMATION

Reversibility limitations of metal exsolution reactions in niobium and nickel co-doped strontium titanate

Moritz L. Weber,*[a,b,c,‡] Yoo Jung Sohn,[c] Regina Dittmann,[b] Rainer Waser,[b,d] Norbert H. Menzler,[d,e] Olivier Guillon,[d,e] Christian Lenser,[c] Slavomír Nemšák,[a,f] and Felix Gunkel[b]

a Advanced Light Source, Lawrence Berkeley National Laboratory, Berkeley, California 94720, United States.
b Peter Gruenberg Institute (PGI-7) and JARA-FIT, Forschungszentrum Juelich GmbH, Wilhelm-Johnen-Straße, 52425 Juelich, Germany
c Institute of Energy and Climate Research (IEK-1), Forschungszentrum Juelich GmbH, Wilhelm-Johnen-Straße, 52425 Juelich, Germany
d Institute for Electronic Materials (IWE 2), RWTH Aachen University, Sommerfeldstraße 18/24, 52074 Aachen, Germany
e Institute of Mineral Engineering (GHI), RWTH Aachen University, Forckenbeckstraße 33, 52074 Aachen, Germany
f Department of Physics, University of California, Davis, California 95616, United States
‡ Present address: Advanced Light Source, Lawrence Berkeley National Labora- tory, Berkeley, California 94720, United States & Peter Gruenberg Institute (PGI- 7) & JARA-FIT, Forschungszentrum Juelich GmbH, Wilhelm-Johnen-Straße, 52425 Juelich, Germany

*Email: mo.weber@fz-juelich.de

Table S1. Exemplary literature references discussing reversibility limitations of metal exsolution reactions. *Exemplary reduction and reoxidation conditions are noted, while several studies applied various annealing conditions.

Composition	Me_{exs}	Sample type	Reduction: *t*, *T*, atm., *	Reoxidation: *t*, *T*, atm., *	Detection	Reversibility	Ref. (main text)
$LaFe_{0.57}Co_{0.38}Pd_{0.05}O_3$	Pd	Powder	1h, 800°C, 10% H_2/ 90% N_2	1h, 800°C, air	XANES, EXAFS	Yes	4
$Sr_2Fe_{1.35}Mo_{0.45}Co_{0.2}O_{6-\delta}$	Fe-Co	Powder	4h, 800°C, 5% H_2 / Ar	4h, 800°C, air	In-situ XRD, in-situ TEM	Yes	11
Ni-doped $Sr_{0.8}Ti_{0.9}Mn_{0.1}O_{3+\delta}$	Ni	Ceramic pellet	20h, 800°C, 5% H_2 / Ar	N/A	N/A	Yes	12
Ni- or Cu-doped $Ca_2Fe_2O_5$	Fe-Ni, Cu	Powder	~1h, 800°C, 5% H_2/ N_2	6h, 850°C, air	XRD, TEM	Yes (Cu) No (Ni)	13
$Sr_{0.93}(Ti_{0.3}Fe_{0.63}Ni_{0.07})O_{3-\delta}$	Fe-Ni	Powder	4h, 700°C, 50% H_2 (humid), *	24h, 700°C, air	NAP-XPS, NAP-XAS, SEM, TEM	Partially	16
$La_{0.3}Sr_{0.7}Cr_{0.3}Fe_{0.6}Co_{0.1}O_{3-\delta}$	Fe-Co	Powder	24h, 800°C, 5% H_2 / Ar	24h, 800°C, air	SEM	Partially	17
$La_xSr_{1-1.5x}Ti_{1-y}Ni_yO_{3-\delta}$	Ni	Powder	N/A, 900°C, 5% H_2 / Ar	N/A, 900°C, air	XRD, SEM	Yes	14
Multiple	Rh, Pd, Pt	Powder, Ceramic pellet	1h, 800°C, 2.5 % H_2 / 7.5 % CO / N_2	1h, 800°C, air	EXAFS, XRD	Yes	15
$LaFe_{0.95}Pd_{0.05}O_{3-\delta}$ $Pd/LaFeO_3$	Pd	Epitaxial thin film	1h, 600°C, 1% H_2/N_2	1h, 800°C, air	TEM, XPS, EDX	No/Partially	46
$CaTi_{0.95}Pt_{0.05}O_{3-\delta}$ $CaTi_{0.95}Rh_{0.05}O_{3-\delta}$	Pt, Rh	Powder, Epitaxial thin film	1h, 800°C, 10% H_2/N_2	1h, 800°C, 20% O_2/N_2	TEM, XPS	No/Partially	18
$La_{0.8}Ce_{0.1}Ni_{0.4}Ti_{0.6}O_3$ $La_{0.7}Ce_{0.1}Co_{0.3}Ni_{0.1}Ti_{0.6}O_3$	Ni, Co-Ni	Ceramic pellet	30h, 550-860°C, 5% H_2 / Ar	During light-off experiment, up to 520°C, CO	SEM, TEM, XPS	No	19
$La_{0.6}Sr_{0.4}FeO_{3-\delta}$	Fe	Thin film	Reduction and re-oxidation by electrochemical polarization		In-situ XRD	No	20

Table 1 summarizes exemplary studies that focus on or mention metal exsolution revesibility, providing information about different aspects of the methodology. Note that different annealing conditions may be applied within the studies, while only exemplary conditions are noted. Furthermore, it is worth noting, that different techniques were applied to detect reversibility in the material systems listed above, which may have a considerable influence on the results. Therefore, we would like to emphasize that we report the conclusions on the reversibility of exsolution reactions in Table 1, although we might reach a different conclusion given the data presented. While efforts have been made to ensure the accuracy and comprehensiveness of the presented data, the authors do not guarantee the completeness of Table 1.

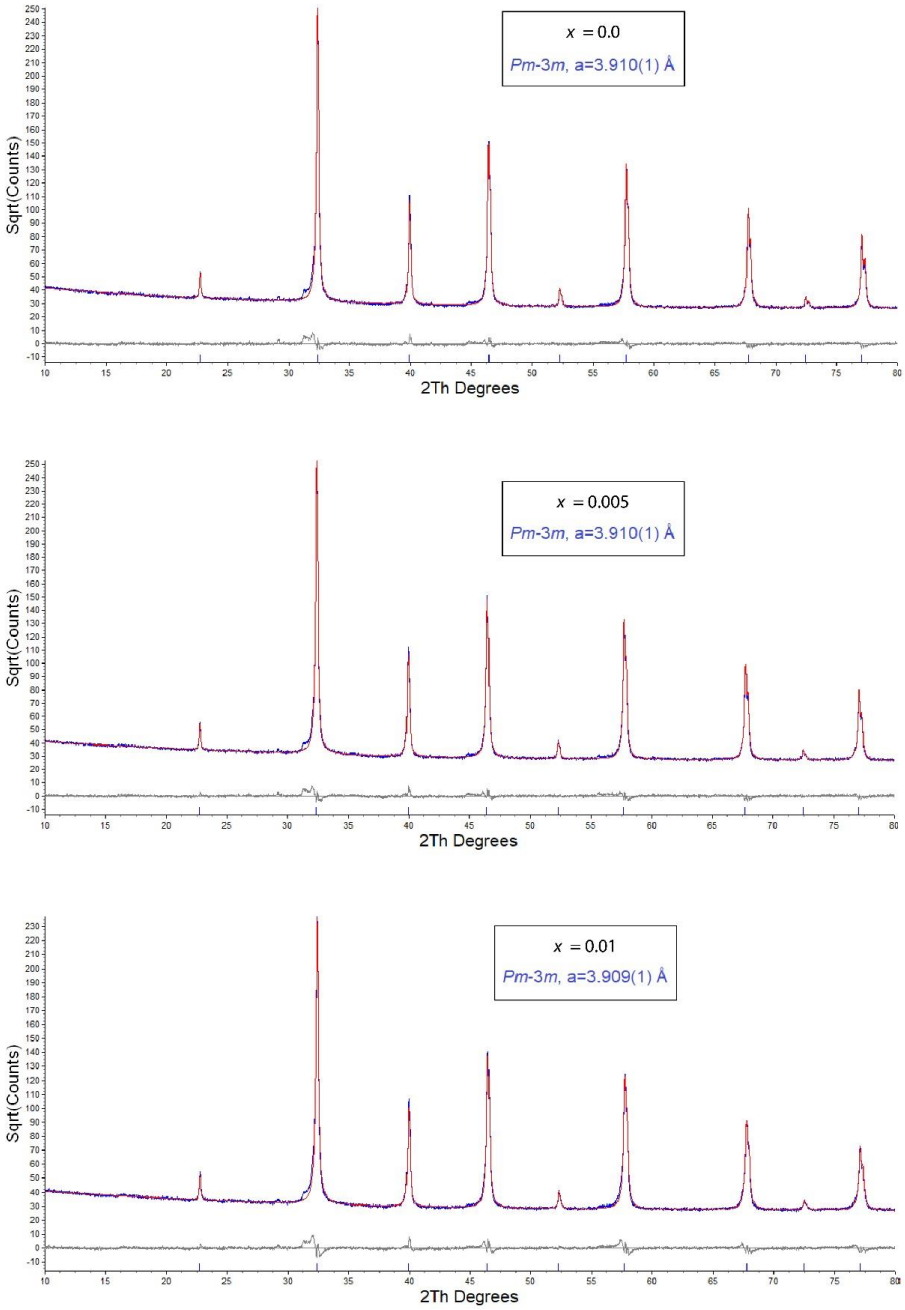

Figure S1. Rietveld refinement of X-ray diffraction patterns obtained from ceramic $SrTi_{0.95-x}Nb_{0.05}Ni_xO_{3-\delta}$ (STNNix) oxide pellets for Ni doping levels in the range between $x = 0.0$-0.01.

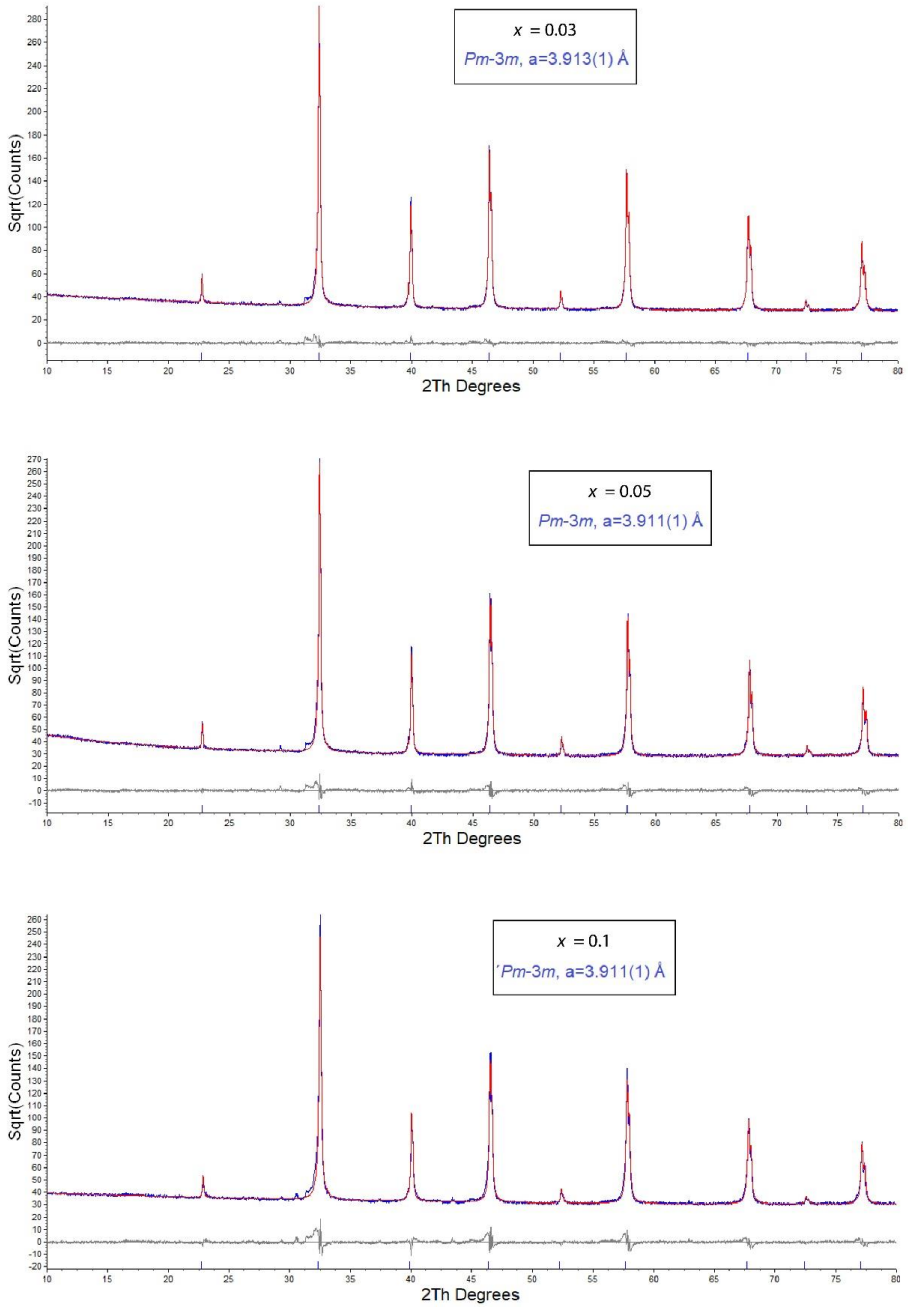

Figure S2. Rietveld refinement of X-ray diffraction patterns obtained from ceramic $SrTi_{0.95-x}Nb_{0.05}Ni_xO_{3-\delta}$ (STNNix) oxide pellets for Ni doping levels in the range between $x = 0.03$-0.1.

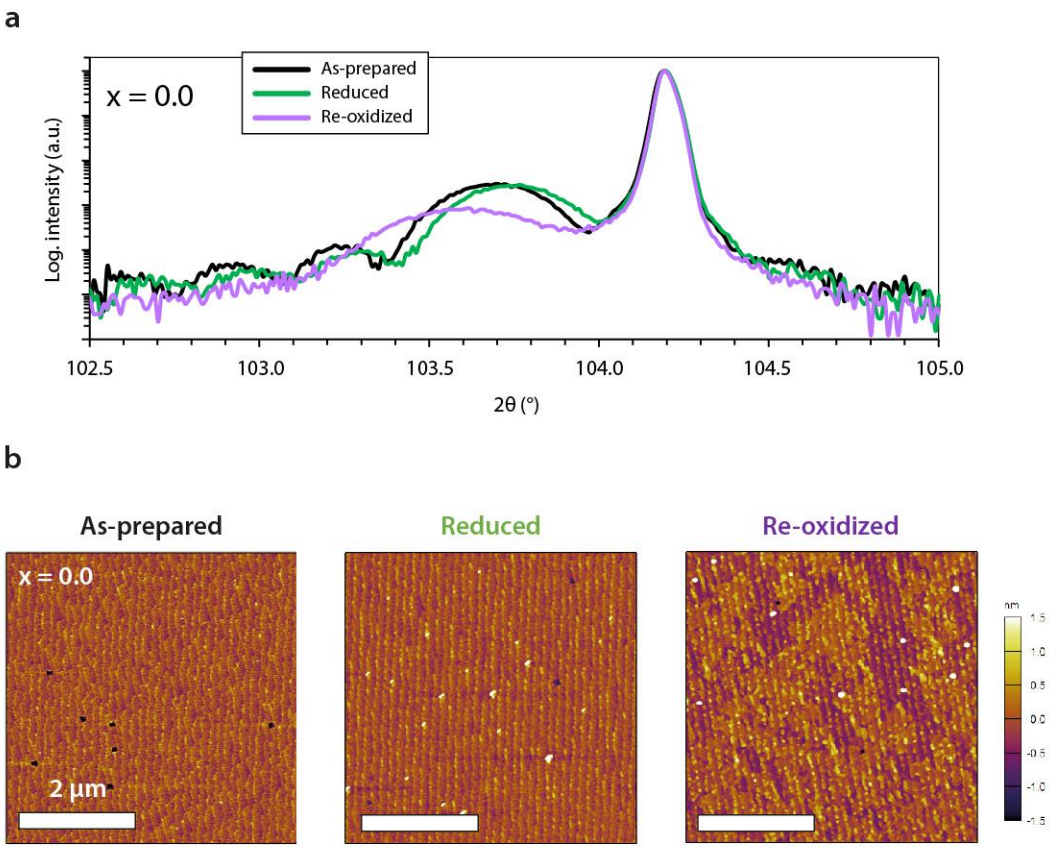

Figure S3. (a) X-ray diffraction analysis and (b) atomic force microscopy of epitaxial STNNix ($x = 0.0$) obtained in the as-prepared, reduced (4% H_2/Ar, $T = 800$°C, 5 h) and reoxidized (air, $T = 800$°C, 5 h) state. The size of the AFM images is 5x5 µm^2, respectively.

Atomic force microscopy imaging and x-ray diffraction analysis obtained from single Nb-doped STO thin films (STNNix with $x = 0.0$) reveals degradation of the perovskite layer under oxidizing conditions. A relaxation in the perovskite *c*-lattice with a similar magnitude as compared to thin films with a low Ni co-doping concentration of $x = 0.005 – 0.03$ (*cf.* Fig 3b main manuscript and Fig. S3 SI) can be observed after thermal reduction, however, a significant broadening of the thin film peak is visible after thermal reoxidation. The broadening of the thin film peak is accompanied by a loss in Laue oscillations in the vicinity of the (004) diffraction peak. These findings indicate a decreased structural coherency of the perovskite layer upon oxidizing treatment. The structural degradation upon reoxidation is associated with the formation of an inhomogeneous surface morphology (Fig. S1b) and may be related to preferential charge compensation of the Nb donors by the introduction of considerable concentrations of Sr vacancies under oxidizing conditions, which may result in the formation of Sr-rich defects such as Ruddlesden-Popper type phases.[1-6]

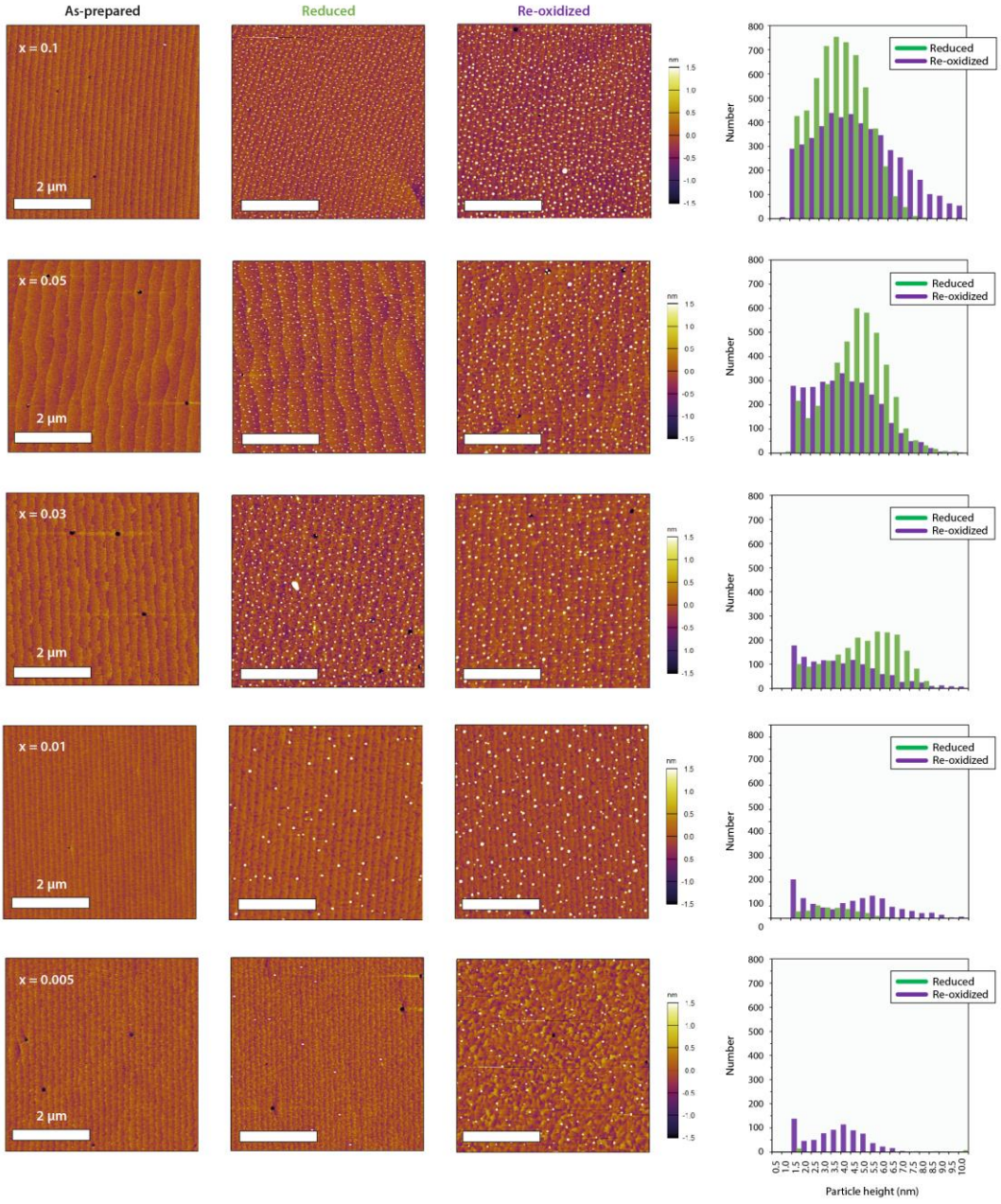

Figure S4. Atomic force microscopy of epitaxial STNNix thin films (x = 0.005 – 0.1). Representative AFM images of the surface morphology of the as-prepared thin films, after thermal reduction (4% H_2/Ar, T = 800°C, 5 h) and after re-oxidation (air, T = 800°C, 5 h) are shown (size 5x5 µm^2): The frequency distribution of the particle height determined on the basis of three 5x5 µm^2 AFM scans is shown on the right, respectively.

Atomic force microscopy images of the STNNix thin films are shown for the as-prepared, reduced and re-oxidized state (Fig. S2), where the frequency distribution of the nanoparticle height for the nanoparticle population obtained from three 5x5 µm^2 scans are given on the right. As can be seen, the as-prepared thin films with x=0.005-0.1 exhibit a smooth surface morphology with a defined step terrace structure. After reduction, exsolved nanoparticles are visible at the surface. For dominant donor-doping of strontium titanate, additional precipitation of SrO islands may be observed during reoxidation in air.

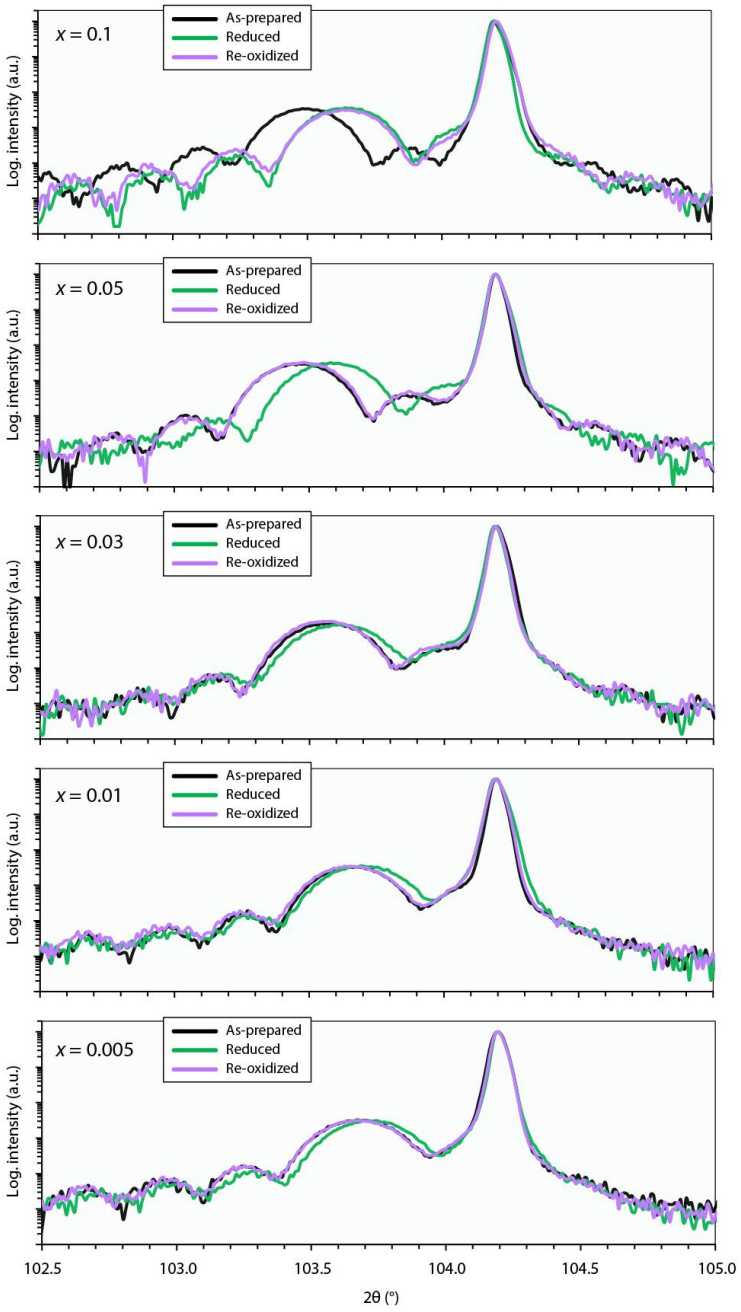

Figure S5. X-ray diffraction analysis of epitaxial STNNix (x = 0.005 – 0.1) thin films in 2θ-ω geometry. The broader (004) diffraction peak of the thin film and the sharp (004) diffraction peak of the substrate are visible. The plot shows data obtained from the as-prepared thin films as well as after reducing thermal treatment (4% H_2/Ar, T = 800°C, 5 h) and after re-oxidation (air, T = 800°C, 5 h). Relative shifts in the (004) thin film diffraction peak indicate changes in the c-lattice parameter.

X-ray diffraction analysis of epitaxial STNNix thin films with x = 0.005 – 0.1 in different redox states reveal differences in the structural properties and the reversibility of bulk structural changes depending on the Ni doping level.

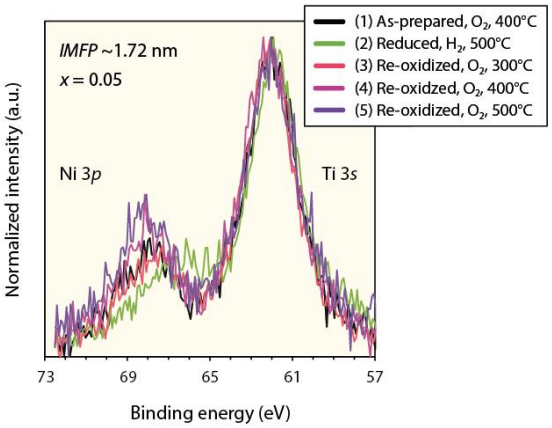

Figure S6. Ambient-pressure X-ray photoelectron spectroscopy of the Ni 3*p*-Ti 3*s* core-level region obtained from STNNix (x = 0.05) with E_{hv} = 900 eV. The electronic signature is compared *in-situ* after consecutive oxidation, reduction and reoxidation steps at different temperatures. The hydrogen and oxygen partial pressure was $p(H_2)$=0.5 mbar and $p(O_2)$=0.5 mbar. The binding energy of all spectra was aligned to *B.E.*(Ti 2*p*) = 458.4 eV and a Shirley-type background was subtracted.

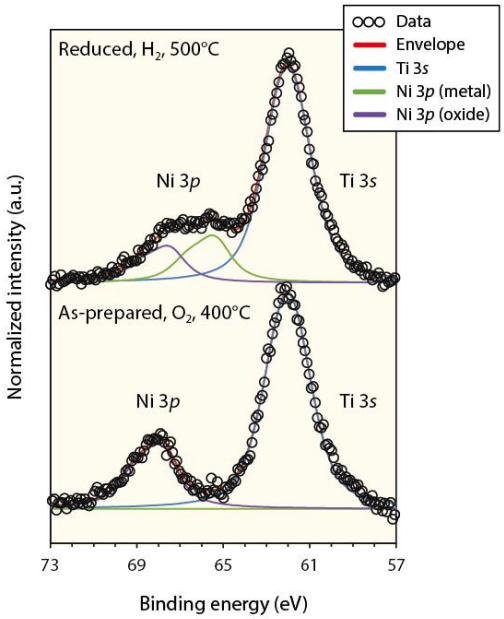

Figure S7. Ambient-pressure X-ray photoelectron spectroscopy of the Ni 3*p*-Ti 3*s* core-level region obtained from STNNix (x = 0.05) with E_{hv} = 680 eV. Representative fitting of the as-prepared state after oxygen treatment to desorb carbon species and after reduction of the sample. The hydrogen and oxygen partial pressure was $p(H_2)$=0.5 mbar and $p(O_2)$=0.5 mbar. The binding energy of all spectra was aligned to *B.E.*(Ti 2*p*) = 458.4 eV and a Shirley-type background was subtracted.

Based on the Ni 3*p*-Ti 3*s* core-level region obtained from the as-prepared sample after an oxygen annealing step, the Ti 3*s* peak was fitted using a Voigt profile and the Ni 3*p* states (oxide component) were fitted using a Voigt doublet. For this purpose, the branching ratio of the Voigt doublet was fixed to the theoretical value for *p*-orbitals *i.e.* 1 : 2 for $3p_{1/2}$: $3p_{3/2}$. Subsequently, the Lorentzian and Gaussian widths for the Ti and Ni peaks as well as the magnitude of spin-orbit-splitting *ΔB.E.* ~1.25 eV of the fitted Ni component was fixed. In addition, the peak position of the fitted Ti 3*s* component was fixed. Using the spectrum obtained from the reduced sample, a second Voigt doublet corresponding to

the metal nickel phase was fitted where a Lorentzian and Gaussian width and spin-orbit-splitting *ΔB.E.* equal to the oxide component was applied. The relative position of the fitted oxide and metal Ni 3*p* components was fixed and the resulting fitting model was applied to all spectra to evaluate the evolution of the peak area ratio.

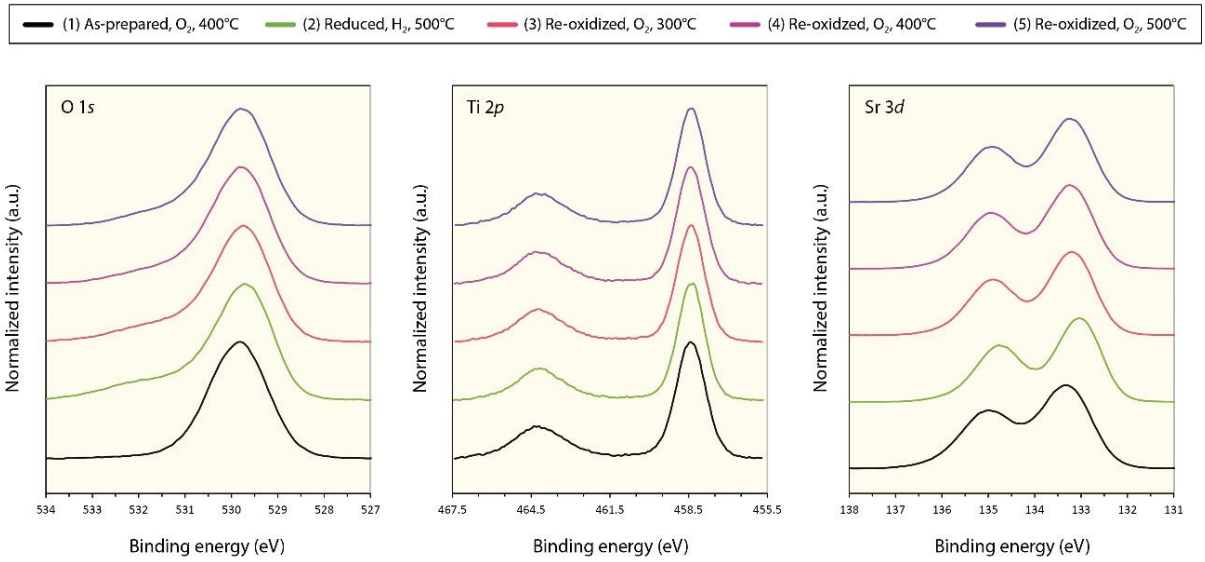

Figure S8. Ambient-pressure X-ray photoelectron spectroscopy of O 1*s*, Ti 2*p* and Sr 3*d* core-levels obtained from the same sample STNNix ($x = 0.05$) with $E_{hv} = 680$ eV as the Ni 3*p*-Ti 3*s* core level region discussed in Figure 3e of the main manuscript. The hydrogen and oxygen partial pressure was $p(H_2)$=0.5 mbar and $p(O_2)$=0.5 mbar. The binding energy of all spectra was aligned to *B.E.*(Ti 2*p*) = 458.4 eV and a Shirley-type background was subtracted.

Figure S8 shows O 1*s*, Ti 2*p* and Sr 3*d* core-levels recorded for the same sample as the Ni 3*p*-Ti 3*s* core-level discussed in Figure 3e of the main manuscript. No significant enrichment of strontium was detected based on the Sr 3*d* / Ti 2*p* peak area ratio, which was determined to be ~2.85 ± 0.05 across all sample states. Furthermore, only small changes in the spectral shape and binding energy were detected during the redox treatment (all spectra aligned with respect to *B.E.*(Ti 2*p*) = 458.4 eV). Here, the evolution of a small shoulder at larger binding energy relative to the perovskite main peak is visible in the O 1*s* after the reduction step. In turn, however, the Sr signature exhibits a single-doublet shape after reduction, where only faint changes in the spectral shape and slight peak broadening may be observed that may indicate a minor change in the chemical environment. It hence is unlikely that the additional O 1*s* shoulder is correlated to Sr segregation. A minor amount of SrO or $Sr(OH)_2$ surface species may be present during sample cleaning in oxidizing atmosphere due to the formation of a space charge region, vanishing upon reducing thermal treatment[7,8].

Moreover, we show Nb 3*d* states for different redox states separately in Fig. S9. Note, Nb 3*d* states were recorded for all but the last oxidation step at $T = 500$°C due to time restrictions. No significant spectral changes can be observed in the Nb 3*d* core-level region.

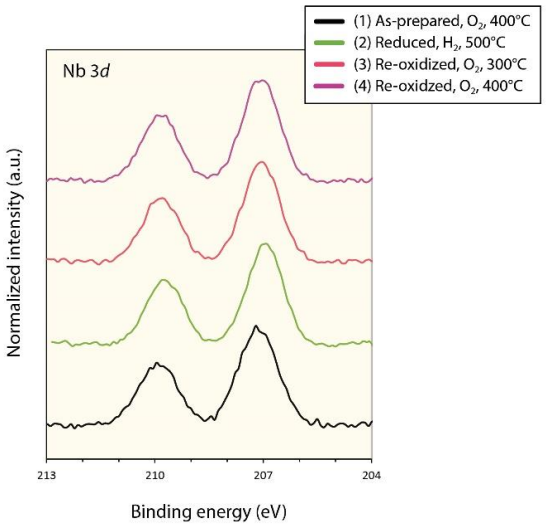

Figure S9. Ambient-pressure X-ray photoelectron spectroscopy of Nb 3*d* core-levels obtained from the same sample STNNix ($x = 0.05$) with $E_{hv} = 680$ eV as the Ni 3*p*-Ti 3*s* core level region discussed in Figure 3e of the main manuscript. The hydrogen and oxygen partial pressure was $p(H_2)$=0.5 mbar and $p(O_2)$=0.5 mbar. The binding energy of all spectra was aligned to *B.E.*(Ti 2*p*) = 458.4 eV and a Shirley-type background was subtracted.

References

(1) Moos, R. and Hardtl, K. H., *Journal of the American Ceramic Society*, 80, 2549–2562 (1997).

(2) Meyer R., Zurhelle, A. F., De Souza, R. A., Waser, R. and Gunkel, F., *Physical Review B*, 94, 115408 (2016).

(3) F. Gunkel, R. Waser, A. H. H. Ramadan, R. A. De Souza, S. Hoffmann-Eifert and R. Dittmann, *Physical Review B*, 93, 24543 (2016).

(4) Blennow, P., Hagen, A., Hansen, K. K., Wallenberg, L. R., Mogensen, M., *Solid State Ionics* 179, 35–36 (2008).

(5) Blennow, P., Hansen, K. K., Wallenberg L. R. and Mogensen, M., *Journal of the European Ceramic Society*, 27, 3609– 3612 (2007).

(6) Balachandran, U. and Eror, N. G., *J. Electrochem. Soc.* 129, 1021 (1982).

(7) M. L. Weber, B. Šmíd, U. Breuer, M.-A. Rose, N. H. Menzler, R. Dittmann, R. Waser, O. Guillon, F. Gunkel and C. Lenser, (under review, pre-print availbale: https://doi.org/10.26434/chemrxiv-2022-v9z6n)

(8) M. Andrä, F. Dvořák, M. Vorokhta, S. Nemšák, V. Matolín, C. M. Schneider, R. Dittmann, F. Gunkel, D. N. Mueller, and R. Waser, *APL materials*, vol. 5, no. 5, p. 056106, (2017).